

Energy Harvesting Technologies

Shashank Priya · Daniel J. Inman
Editors

Energy Harvesting Technologies

 Springer

Editors

Shashank Priya
Virginia Tech
Center for Intelligent Material Systems
and Structures
Department of Mechanical Engineering
304A Holden Hall
Blacksburg, VA 24061
spriya@mse.vt.edu

Daniel J. Inman
Virginia Tech
Center for Intelligent Material Systems
and Structures
Department of Mechanical Engineering
310 Durham Hall
Blacksburg, VA 24061
dinman@vt.edu

ISBN 978-0-387-76463-4

e-ISBN 978-0-387-76464-1

DOI 10.1007/978-0-387-76464-1

Library of Congress Control Number: 2008934452

© Springer Science+Business Media, LLC 2009

All rights reserved. This work may not be translated or copied in whole or in part without the written permission of the publisher (Springer Science+Business Media, LLC, 233 Spring Street, New York, NY 10013, USA), except for brief excerpts in connection with reviews or scholarly analysis. Use in connection with any form of information storage and retrieval, electronic adaptation, computer software, or by similar or dissimilar methodology now known or hereafter developed is forbidden.

The use in this publication of trade names, trademarks, service marks, and similar terms, even if they are not identified as such, is not to be taken as an expression of opinion as to whether or not they are subject to proprietary rights.

Printed on acid-free paper

springer.com

Preface

Energy harvesting materials and systems have emerged as a prominent research area and continues to grow at rapid pace. A wide range of applications are targeted for the harvesters, including distributed wireless sensor nodes for structural health monitoring, embedded and implanted sensor nodes for medical applications, recharging the batteries of large systems, monitoring tire pressure in automobiles, powering unmanned vehicles, and running security systems in household conditions. Recent development includes the components and devices at micro–macro scales covering materials, electronics, and integration. The growing demand for energy harvesters has motivated the publication of this book to present the current state of knowledge in this field.

The book is addressed to students, researchers, application engineers, educators, developers, and producers of energy harvesting materials and systems. The chapters mainly consist of technical reviews, discussions, and basic knowledge in the design and fabrication of energy harvesting systems. It brings the leading researchers in the world in the field of energy harvesting and associated fields on to one platform to provide a comprehensive overview of the fundamentals and developments. The book has good mix of researchers from academics, industry, and national laboratories. All the important energy harvesting technologies including piezoelectric, inductive, thermoelectric, and microbatteries are addressed by the leading authors. Furthermore, the book covers the principles and design rules of the energy harvesting circuits in depth. The chapters on demonstrated applications of the energy harvesting-based technologies will allow readers to conceptualize the promise of the field.

The first section in the book provides discussions on background, theoretical models, equivalent circuit models, lumped models, distributed models, and basic principles for design and fabrication of bulk and MEMS-based vibration-based energy harvesting systems. The second section addresses the theory and design rules required for the fabrication of the efficient electronics. The third section discusses the progress in the field of thermoelectric energy harvesting systems. The fourth section addresses the important subject of storage systems. The fifth section describes some of the prototype demonstrations reported so far utilizing energy harvesting. The sixth section reports some initial standards for vibration energy harvesting being formalized by a nationwide committee consisting of researchers from academia and

industry. This standard will lay the basic rules for conducting and reporting the research on vibration energy harvesting. The publication of this standard follows the annual energy harvesting workshop. Fourth workshop in this series will be held at Virginia Tech on January 28–29, 2009. It is worthwhile to mention here that this workshop in the last 3 years has grown in size and numbers with growing participation from academia and industry.

The chapters published here are mostly the invited technical submissions from the authors. The editors did not make any judgment on the quality and organization of the text in the chapters and it was mostly left to the decision of the authors. In this regard, the editors do not accept the responsibility for any technical errors present in the chapters and those should be directly discussed with the authors of the relevant chapter.

It was an honor editing this book consisting of contributions from knowledgeable and generous colleagues. Thanks to all the authors for their timely assistance and cooperation during the course of this book. Without their continual support, this work would not have been possible. We hope that readers will find the book informative and instructive and provide suggestions and comments to further improve the text in eventual second edition.

Blacksburg, VA

Shashank Priya and Dan J. Inman

Contents

Part I Piezoelectric and Electromagnetic Energy Harvesting

1 Piezoelectric Energy Harvesting	3
Hyunuk Kim, Yonas Tadesse, and Shashank Priya	
1.1 Energy Harvesting Basics	4
1.2 Case Study: Piezoelectric Plates Bonded to Long Cantilever Beam with tip mass	7
1.3 Piezoelectric Materials	9
1.3.1 Piezoelectric Polycrystalline Ceramics	10
1.3.2 Piezoelectric Single Crystal Materials	11
1.3.3 Piezoelectric and Electrostrictive Polymers	13
1.3.4 Piezoelectric Thin Films	14
1.4 Piezoelectric Transducers	16
1.5 Meso-macro-scale Energy Harvesters	16
1.5.1 Mechanical Energy Harvester Using Laser Micromachining	16
1.5.2 Mechanical Energy Harvester Using Piezoelectric Fibers	20
1.6 Piezoelectric Microgenerator	21
1.6.1 Piezoelectric Microcantilevers	21
1.7 Energy Harvesting Circuits	24
1.8 Strategies for Enhancing the Performance of Energy Harvester	26
1.8.1 Multi-modal Energy Harvesting	26
1.8.2 Magnetoelectric Composites	29
1.8.3 Self-Tuning	31
1.8.4 Frequency Pumping	32
1.8.5 Wide-Bandwidth Transducers	33
1.9 Selected Applications	33
1.9.1 Border Security Sensors	33
1.9.2 Biomedical Applications	35
1.10 Summary	35
References	36

2	Electromechanical Modeling of Cantilevered Piezoelectric Energy Harvesters for Persistent Base Motions	41
	Alper Erturk and Daniel J. Inman	
2.1	Introduction	41
2.2	Amplitude-Wise Correction of the Lumped Parameter Model . . .	44
2.2.1	Uncoupled Lumped Parameter Base Excitation Model . .	45
2.2.2	Uncoupled Distributed Parameter Base Excitation Model	46
2.2.3	Correction Factors for the Lumped Parameter Model . . .	50
2.2.4	Correction Factor in the Piezoelectrically Coupled Lumped Parameter Equations	55
2.3	Coupled Distributed Parameter Models and Closed-Form Solutions	57
2.3.1	Modeling Assumptions	57
2.3.2	Mathematical Background	58
2.3.3	Unimorph Configuration	61
2.3.4	Bimorph Configurations	64
2.3.5	Single-Mode Electromechanical Equations	67
2.3.6	Experimental Validation	69
	References	76
3	Performance Evaluation of Vibration-Based Piezoelectric Energy Scavengers	79
	Yi-Chung Shu	
3.1	Introduction	79
3.1.1	Piezoelectric Bulk Power Generators	81
3.1.2	Piezoelectric Micro Power Generators	82
3.1.3	Conversion Efficiency and Electrically Induced Damping	83
3.1.4	Power Storage Circuits	84
3.2	Approach	84
3.2.1	Standard AC–DC Harvesting Circuit	84
3.2.2	SSHI-Harvesting Circuit	89
3.3	Results	92
3.3.1	Standard Interface	92
3.3.2	SSHI Interface	96
3.4	Conclusion	100
	References	100
4	Piezoelectric Equivalent Circuit Models	107
	Björn Richter, Jens Twiefel and Jörg Wallaschek	
4.1	Model Based Design	107
4.1.1	Basic Configurations of Piezoelectric Generators	108
4.2	Linear Constitutive Equations for Piezoelectric Material	108

4.3	Piezoelectric Equivalent Circuit Models for Systems with Fixed Mechanical Boundary	109
4.3.1	Quasi-Static Regime	110
4.3.2	Single Degree of Freedom Model for Dynamic Regime	111
4.3.3	Multi-Degree of Freedom Model for Dynamic Regime	113
4.3.4	Experimental Parameter Identification	114
4.3.5	Case Study	116
4.4	Analytical Determination of the Parameters of the Equivalent Circuit Models	117
4.4.1	General Procedure for Analytical Bimorph Model	118
4.4.2	Determination of the Parameters of the Piezoelectric Equivalent Circuit Models using the Analytical Model	119
4.5	Equivalent Circuit Model for Base Excited Piezoelectric Systems	120
4.6	Overall PEG System Analyses Using Piezoelectric Equivalent Circuit Models	121
4.6.1	Piezoelectric Equivalent Circuit Model with Electrical Load	122
4.6.2	Analysis of the Maximum Power Output	122
4.6.3	Experimental Validation of the Piezoelectric Equivalent Circuit Model for Base Excitation	124
4.6.4	Effect of Geometry	125
4.6.5	Modeling of the Coupling Between the PEG and Its Excitation Source, Additional Degrees of Freedom	126
4.7	Summary	127
	References	128
5	Electromagnetic Energy Harvesting	129
	Stephen P Beeby and Terence O'Donnell	
5.1	Introduction	129
5.2	Basic Principles	130
5.3	Wire-Wound Coil Properties	132
5.4	Micro-Fabricated Coils	134
5.5	Magnetic Materials	136
5.6	Scaling of Electromagnetic Vibration Generators	139
5.7	Scaling of Electromagnetic Damping	142
5.8	Maximising Power from an EM Generator	145
5.9	Review of Existing Devices	146
5.10	Microscale Implementations	146
5.11	Macro-Scale Implementations	151

5.12	Commercial Devices	154
5.13	Conclusions	158
	References	159

Part II Energy Harvesting Circuits and Architectures

6	On the Optimal Energy Harvesting from a Vibration Source Using a Piezoelectric Stack	165
	Jamil M. Renno, Mohammed F. Daqaq and Daniel J. Inman	
6.1	Introduction	166
6.2	One-dimensional Electromechanical Analytic Model	168
6.3	Power Optimization	172
6.4	Optimality of the Parallel- <i>RL</i> Circuit	173
	6.4.1 The Purely Resistive Circuit	175
	6.4.2 The Parallel- <i>RL</i> Circuit	183
6.5	The Series- <i>RL</i> Circuit	188
	6.5.1 Optimality Results for Series <i>RL</i> -Circuit	189
6.6	Conclusions	192
	References	192
7	Energy Harvesting Wireless Sensors	195
	S.W. Arms, C.P. Townsend, D.L. Churchill, M.J. Hamel, M. Augustin, D. Yeary, and N. Phan	
7.1	Introduction	195
7.2	Background	196
7.3	Tracking Helicopter Component Loads with Energy Harvesting Wireless Sensors	196
7.4	Monitoring Large Bridge Spans with Solar-Powered Wireless Sensors	204
7.5	About MicroStrain Inc.	207
	References	207
8	Energy Harvesting using Non-linear Techniques	209
	Daniel Guyomar, Claude Richard, Adrien Badel, Elie Lefeuvre and Mickaël Lallart	
8.1	Introduction	210
8.2	Introduction to Nonlinear Techniques and their Application to Vibration Control	211
	8.2.1 Principles	211
8.3	Energy Harvesting Using Nonlinear Techniques in Steady-State Case	221
	8.3.1 Principles	222
	8.3.2 Analysis Without Induction of Vibration Damping	223

8.3.3	Damping Effect	227
8.3.4	Experimental Validation	232
8.4	Energy Harvesting in Pulsed Operation	236
8.4.1	SSHI Technique	237
8.4.2	Performance Comparison	243
8.4.3	Experimental Validation	244
8.5	Other Nonlinear Energy Harvesting Techniques	247
8.5.1	Series SSHI Technique	247
8.5.2	Theoretical Development with Damping Effect	251
8.5.3	Synchronous Electric Charge Extraction (SECE) Technique	254
8.5.4	Experimental Validation	258
8.6	Energy Harvesting Techniques under Broadband Excitation	262
8.6.1	Multimodal Vibrations	263
8.6.2	Random Vibrations	263
8.7	Conclusion	265
	References	265
9	Power Sources for Wireless Sensor Networks	267
	Dan Steingart	
9.1	Introduction	267
9.2	Primary Batteries	271
9.3	Energy harvesting	273
9.3.1	Energy Harvesting versus Energy Scavenging	273
9.3.2	Photonic Methods	274
9.3.3	Vibrational Methods	276
9.3.4	Thermal Methods	279
9.4	Alternative Methods	280
9.4.1	RF Power	280
9.4.2	Radioactive Sources	281
9.5	Power Conversion	281
9.6	Energy Storage	281
9.7	Examples	282
9.7.1	Sensors in a Cave	282
9.7.2	Sensors in an Industrial Plant	282
9.7.3	Sensors in Nature	283
9.8	Conclusion	284
	References	284
10	Harvesting Microelectronic Circuits	287
	Gabriel A. Rincón-Mora	
10.1	Harvesting Sources	288
10.1.1	Energy and Power	288
10.1.2	Energy Sources	289

10.2	Power Conditioning	293
10.2.1	Microsystem	293
10.2.2	Linear DC–DC Converters	295
10.2.3	Switching DC–DC Converters	296
10.2.4	Switching AC–DC Converters	303
10.2.5	Comparison	304
10.3	Power Losses	305
10.3.1	Conduction Losses	306
10.3.2	Switching Losses	310
10.3.3	Quiescent Losses	312
10.3.4	Losses Across Load	313
10.4	Sample System: Electrostatic Harvester	314
10.4.1	Harvesting Current	315
10.4.2	Trickle Charging Scheme	315
10.4.3	Harvesting Microelectronic Circuit	317
10.5	Summary	321

Part III Thermoelectrics

11	Thermoelectric Energy Harvesting	325
	G. Jeffrey Snyder	
11.1	Harvesting Heat	325
11.2	Thermoelectric Generators	326
11.3	Design of a Thermoelectric Energy Harvester	328
11.4	General Considerations	328
11.5	Thermoelectric Efficiency	328
11.6	Matched Thermal Resistance	330
11.7	Heat Flux	332
11.8	Matching Thermoelectrics to Heat Exchangers	332
11.8.1	Thin Film Devices	334
11.9	Additional Considerations	335
11.10	Summary	335
	References	335
12	Optimized Thermoelectrics For Energy Harvesting Applications	337
	James L. Bierschenk	
12.1	Introduction	337
12.2	Basic Thermoelectric Theory	338
12.3	Device Effective ZT	341
12.4	System Level Design Considerations	343
12.5	System Optimization for Maximum Power Output	344
12.6	Design Considerations for Maximizing Voltage Output	347
12.7	Conclusions	350
	References	350

Part IV Microbatteries

13 Thin Film Batteries for Energy Harvesting 355
 Nancy J. Dudney

13.1 Introduction 355

13.2 Structure, Materials, and Fabrication of TFB 356

13.3 Performance of TFBs 358

 13.3.1 Energy and Power 358

 13.3.2 Charging 360

 13.3.3 Cycle-Life and Shelf-Life 360

 13.3.4 High and Low Temperature Performance 362

13.4 Outlook and Summary 362

References 362

14 Materials for High-energy Density Batteries 365
 Arumugam Manthiram

14.1 Introduction 365

14.2 Principles of Lithium–Ion Batteries 366

14.3 Cathode Materials 369

 14.3.1 Layered Oxide Cathodes 370

 14.3.2 Spinel Oxide Cathodes 374

 14.3.3 Olivine Oxide Cathodes 377

14.4 Anode Materials 380

14.5 Conclusions 381

References 382

Part V Selected Applications of Energy Harvesting Systems

15 Feasibility of an Implantable, Stimulated Muscle-Powered Piezoelectric Generator as a Power Source for Implanted Medical Devices 389
 B.E. Lewandowski, K. L. Kilgore, and K.J. Gustafson

15.1 Introduction 389

15.2 Generator Driven by Muscle Power 390

15.3 Selection of Mechanical-to-Electrical Conversion Method 393

15.4 Properties of Piezoelectric Material Relevant to the Generator System 395

15.5 Predicted Output Power of Generator 398

15.6 Steps Towards Reduction to Practice 400

15.7 Conclusion 401

References 402

16	Piezoelectric Energy Harvesting for Bio-MEMS Applications	405
	William W. Clark and Changki Mo	
16.1	Introduction	405
16.2	General Expression for Harvesting Energy with Piezoelectric Device	407
16.3	Unimorph Diaphragm in Bending	410
16.3.1	Simply Supported Unimorph Diaphragm that Is Partially Covered with Piezoelectric Material	416
16.3.2	Clamped Unimorph Diaphragm that is Partially Covered with Piezoelectric Material	420
16.4	Simulation Results and Analysis	426
16.5	Conclusions	429
	References	430
17	Harvesting Energy from the Straps of a Backpack Using Piezoelectric Materials	431
	Henry A. Sodano	
17.1	Introduction	431
17.2	Model of Power-Harvesting System	436
17.2.1	Experimental Testing of Piezoelectric Strap	439
17.2.2	Results and Model Validation	443
17.2.3	Backpack Power Prediction	444
17.3	Energy Harvesting Using a Mechanically Amplified Piezoelectric Stack	448
17.3.1	Model and Experimental Validation of Energy Harvesting System	450
17.3.2	Results and Model Validation	452
17.3.3	Backpack Power Prediction	456
17.4	Conclusions	457
	References	458
18	Energy Harvesting for Active RF Sensors and ID Tags	459
	Abhiman Hande, Raj Bridgelall, and Dinesh Bhatia	
18.1	Introduction	460
18.2	RFID Tags	461
18.2.1	Passive RFID	462
18.2.2	Battery-Assisted Passive (BAP) RFID	463
18.2.3	Active RFID	463
18.3	RFID Operation and Power Transfer	466
18.4	Battery Life	467
18.5	Operational Characteristics of RF Sensors and ID Tags	468
18.6	Why EH Is Important?	470
18.7	EH Technologies and Related Work	471

18.8	EH Design Considerations	473
18.8.1	Energy Storage Technologies	473
18.8.2	Energy Requirements and Power Management Issues . . .	474
18.8.3	Vibrational Energy Harvesting	475
18.8.4	Solar Energy Harvesting	479
18.9	Relevant Circuits and Systems	483
18.9.1	AC–DC Rectifier	483
18.9.2	DC–DC Switch-Mode Converters	484
18.10	Future Directions and Scope	487
18.11	Conclusions	488
	References	488
19	Powering Wireless SHM Sensor Nodes through Energy Harvesting	493
	Gyuhae Park, Kevin M. Farinholt, Charles R. Farrar, Tajana Rosing, and Michael D. Todd	
19.1	Introduction	493
19.2	Sensing System Design for SHM	494
19.3	Current SHM Sensor Modalities	495
19.4	Energy Optimization Strategies Associated with Sensing Systems	496
19.4.1	Dynamic Voltage Scaling	497
19.4.2	Dynamic Power Management	498
19.5	Applications of Energy Harvesting to SHM	500
19.6	Future Research Needs and Challenges	503
19.7	Conclusion	505
	References	505
A	Appendix A First Draft of Standard on Vibration Energy Harvesting	507
A.1	Potential Vibration Sources for Energy Harvesting	508
A.2	Parameters Required to Describe the Source	509
A.3	Theoretical Models Used to Describe the Vibration Energy Harvesting	509
A.3.1	Williams-Yates Model	509
A.3.2	Erturk–Inman Model	510
A.4	Characterization of Vibration Energy Harvester	511
A.5	Characterization of the Conditioning Circuit	512
	References	512
Index	515

Contributors

S.W. Arms

MicroStrain, Inc., 459 Hurricane Lane, Williston, Vermont 05495, USA,
swarms@microstrain.com

M. Augustin

MicroStrain, Inc., 310 Hurricane Lane, Williston, Vermont 05495, USA,
MAugustin@bellhelicopter.textron.com

Adrien Badel

Ferroelectricity and Electrical Engineering Laboratory (LGEF), National
Institute of Applied Science Lyon (INSA de Lyon), 69621 Villeurbanne, France,
adrien.badel@insa-lyon.fr

Stephen P Beeby

University of Southampton, Highfield, Southampton, SO17 1BJ, UK,
spb@ecs.soton.ac.uk

Dinesh Bhatia

Electrical Engineering Department, University of Texas at Dallas, 800 W Campbell
Road, Richardson, TX 75080, USA, dinesh@utdallas.edu

James L. Bierschenk

Marlow Industries, Inc., 10451 Vista Park Road, Dallas TX 75238, USA,
JBIERSCHENK@marlow.com

Raj Bridgelall

Axcess International Inc, 3208 Commander Drive, Carrollton, TX 75006, USA,
r.bridgelall@axcessinc.com

D.L. Churchill

MicroStrain, Inc., 310 Hurricane Lane, Williston, Vermont 05495, USA,
tlbarrows@microstrain.com

William W. Clark

University of Pittsburgh, Pittsburgh, PA 15261, 412-624-9794, USA,
wclark@pitt.edu, bluetick@pitt.edu

Mohammed F. Daqaq

Department of Mechanical Engineering, Clemson University, daqaq@clemson.edu

Nancy J. Dudney

Material Science and Technology Division, Oak Ridge National Laboratory, Oak Ridge, TN, USA, dudneyj@ornl.gov

Alper Erturk

Center for Intelligent Material Systems and Structures, Department of Engineering Science and Mechanics, Virginia Polytechnic Institute and State University, Blacksburg, VA 24061, USA, erturk@vt.edu

Kevin M. Farinholt

The Engineering Institute, Los Alamos National Laboratory, Los Alamos, New Mexico 87545, USA, farinholt@lanl.gov

Charles R. Farrar

The Engineering Institute, Los Alamos National Laboratory, Los Alamos, New Mexico 87545, USA, farrar@lanl.gov

K. J. Gustafson

Case Western Reserve University, Department of Biomedical Engineering, Cleveland, OH 44106, USA; Louis Stokes Cleveland Department of Veterans Affairs Medical Center, Cleveland, OH 44106, USA

Daniel Guyomar

Laboratoire de Génie Electrique et de Ferroélectricité, INSA Lyon, France, daniel.guyomar@insa-lyon.fr

M.J. Hamel

MicroStrain, Inc., 310 Hurricane Lane, Williston, Vermont 05495, USA

Abhiman Hande

Electrical Engineering Department, University of Texas at Dallas, 800 W Campbell Road, Richardson, TX 75080, USA; Texas MicroPower Inc., 18803 Fortson Ave, Dallas Texas, 75252, USA, ahande@texasmicropower.com

Daniel J. Inman

Center for Intelligent Material Systems and Structures, Department of Mechanical Engineering, Virginia Polytechnic Institute and State University, Blacksburg, VA 24061, USA, dinman@vt.edu

K. L. Kilgore

Case Western Reserve University, Department of Biomedical Engineering, Cleveland, OH 44106, USA; Metro Health Medical Center, Cleveland, OH 44109, USA; Louis Stokes Cleveland Department of Veterans Affairs Medical Center, Cleveland, OH 44106, USA

Hyunuk Kim

Center for Intelligent Material Systems and Structures, Center for Energy Harvesting Materials and Systems, Virginia Tech, Blacksburg, VA 24061, USA.

Mickaël Lallart

Laboratoire de Génie Electrique et de Ferroélectricité, INSA Lyon, France, mickael.lallart@insa-lyon.fr

Elie Lefevre

Laboratoire de Génie Electrique et de Ferroélectricité, INSA Lyon, France

B. E. Lewandowski

NASA Glenn Research Center, Bioscience and Technology Branch, Cleveland, OH 44135, USA; Case Western Reserve University, Department of Biomedical Engineering, Cleveland, OH 44106, USA, beth.e.lewandowski@nasa.gov

Arumugam Manthiram

Electrochemical Energy Laboratory, Materials Science and Engineering Program, The University of Texas at Austin, Austin, TX 78712, USA, rmanth@mail.utexas.edu

Changki Mo

University of Pittsburgh, Pittsburgh, PA 15261, 412-624-9794, USA

Dr Terence O'Donnell

Tyndall National Institute, Lee Maltings, Prospect Row, Cork, Ireland

Gyuhae Park

The Engineering Institute, Los Alamos National Laboratory, Los Alamos, New Mexico 87545, USA, gpark@lanl.gov

N. Phan

MicroStrain, Inc., 310 Hurricane Lane, Williston, Vermont 05495, USA

Shashank Priya

Center for Intelligent Material Systems and Structures, Center for Energy Harvesting Materials and Systems, Virginia Tech, Blacksburg, VA 24061, USA, spriya@mse.vt.edu

Jamil M. Renno

Center for Intelligent Material Systems and Structures, Virginia Polytechnic Institute and State University, VA, USA, renno@vt.edu

Claude Richard

INSA Lyon, France

Björn Richter

Heinz Nixdorf Institute, University of Paderborn, 33102 Paderborn, Germany

Gabriel A. Rincón-Mora

School of Electrical and Computer Engineering, Georgia Institute of Technology, Atlanta, GA 30332-0250, USA, rincon-mora@ece.gatech.edu

Tajana Rosing

Jacobs of School of Engineering, University of California, San Diego, La Jolla, CA 92093, USA

Yi-Chung Shu

Institute of Applied Mechanics, National Taiwan University, Taipei 106, Taiwan, ROC, yichung@spring.iam.ntu.edu.tw

G. Jeffrey Snyder

Materials Science, California Institute of Technology, 1200 East California, Boulevard, Pasadena, California 91125, USA, jsnyder@caltech.edu

Henry A. Sodano

Department of Mechanical Engineering – Engineering Mechanics, Michigan Technological University, Houghton, MI 49931-1295, USA, Henry.Sodano@asu.edu

Dan Steingart

Department of Chemical Engineering, City College of New York, 140th Street at Convent Avenue, New York, NY 10031, USA, dan.steingart@gmail.com

Yonas Tadesse

Center for Intelligent Material Systems and Structures, Center for Energy Harvesting Materials and Systems, Virginia Tech, Blacksburg, VA 24061, USA, yonas@vt.edu

Michael D. Todd

Jacobs of School of Engineering, University of California, San Diego, La Jolla, CA 92093, USA, mdt@ucsd.edu

C.P. Townsend

MicroStrain, Inc., 310 Hurricane Lane, Williston, Vermont 05495, USA

Jens Twiefel

Institute of Dynamics and Vibration Research, Leibniz University Hannover, 30167 Hannover, Germany, twiefel@ids.uni-hannover.de

Jörg Wallaschek

Institute of Dynamics and Vibration Research, Leibniz University Hannover, 30167 Hannover, Germany, wallaschek@ids.uni-hannover.de

D. Yeary

MicroStrain, Inc., 310 Hurricane Lane, Williston, Vermont 05495, USA, Ryeary@bellhelicopter.textron.com

Part I
Piezoelectric and Electromagnetic
Energy Harvesting

Chapter 1

Piezoelectric Energy Harvesting

Hyunuk Kim, Yonas Tadesse, and Shashank Priya

Abstract This chapter provides the introductory information on piezoelectric energy harvesting covering various aspects such as modeling, selection of materials, vibration harvesting device design using bulk and MEMS approach, and energy harvesting circuits. All these characteristics are illustrated through selective examples. A simple step-by-step procedure is presented to design the cantilever beam based energy harvester by incorporating piezoelectric material at maximum stress points in first and second resonance modes. Suitable piezoelectric material for vibration energy harvesting is characterized by the large magnitude of product of the piezoelectric voltage constant (g) and the piezoelectric strain constant (d) given as $(d \cdot g)$. The condition for obtaining large magnitude of $d \cdot g$ has been shown to be as $|d| = \varepsilon^n$, where ε is the permittivity of the material and n is a material parameter having lower limit of 0.5. The material can be in the form of polycrystalline ceramics, textured ceramics, thin films, and polymers. A brief coverage of various material systems is provided in all these categories. Using these materials different transducer structures can be fabricated depending upon the desired frequency and vibration amplitude such as multilayer, MFC, bimorph, amplified piezoelectric actuator, QuickPack, rainbow, cymbal, and moonie. The concept of multimodal energy harvesting is introduced at the end of the chapter. This concept provides the opportunity for further enhancement of power density by combining two different energy-harvesting schemes in one system such that one assists the other.

In last decade, the field of energy harvesting has increasingly become important as evident from the rising number of publications and product prototypes. Several excellent review articles have been published on this topic covering wide variety of mechanisms and techniques (Priya 2007, Anton and Sodano 2007, Beeby et al. 2006, Roundy and Wright 2004, Sodano et al. 2004). At the same time, several applications have been projected for the energy harvesters covering wide range of civilian and defense components. Out of these different applications, the prominent

H. Kim (✉)

Center for Intelligent Material Systems and Structures, Center for Energy Harvesting Materials and Systems, Virginia Tech, Blacksburg, VA 24061.

use of harvester is to power the wireless sensor node. A major challenge in the implementation of multi-hop sensor networks is supplying power to the nodes (Gonzalez et al. 2002). Powering of the densely populated nodes in a network is a critical problem due to the high cost of wiring or replacing batteries. In many cases, these operations may be prohibited by the infrastructure (Raghunathan et al. 2005, Paradiso and Starner 2005).

Outdoor solar energy has the capability of providing power density of $15,000 \mu\text{W}/\text{cm}^3$ which is about two orders of magnitudes higher than other sources. However, solar energy is not an attractive source of energy for indoor environments as the power density drops down to as low as $10\text{--}20 \mu\text{W}/\text{cm}^3$. Mechanical vibrations ($300 \mu\text{W}/\text{cm}^3$) and air flow ($360 \mu\text{W}/\text{cm}^3$) are the other most attractive alternatives (Roundy et al. 2005, Roundy et al. 2003, Starner and Paradiso 2004). In addition to mechanical vibrations, stray magnetic fields that are generated by AC devices and propagate through earth, concrete, and most metals, including lead, can be the source of electric energy. The actual AC magnetic field strengths encountered within a given commercial building typically range from under 0.2 mG in open areas to several hundred near electrical equipment such as cardiac pace makers, CRT displays, oscilloscopes, motor vehicles (approximately up to 5 G max); computers, magnetic storage media, credit card readers, watches (approximately up to 10 G max); magnetic power supply, liquid helium monitor (approximately up to 50 G max); magnetic wrenches, magnetic hardware, and other machinery (approximately up to 500 G max). AC magnetic fields decrease naturally in intensity as a function of distance (d) from the source. The rate of decrease, however, can vary dramatically depending on the source. For example, magnetic fields from motors, transformers, and so on, decrease very quickly ($1/d^3$), while circuits in a typical multi-conductor circuit decay more slowly ($1/d^2$). Magnetic fields from “stray” current on water pipes, building steel, and so on, tend to decay much more slowly ($1/d$). The other important sources of energy around us are radio frequency waves and acoustic waves.

This chapter provides the introductory information on piezoelectric energy harvesting covering various aspects such as modeling, materials, device design, circuits, and example applications. All of these aspects have been discussed in much detail in the subsequent chapters.

1.1 Energy Harvesting Basics

Vibration of a rigid body can be caused by several factors such as unbalanced mass in a system, tear and wear of materials and can occur in almost all dynamical systems. The characteristic behavior is unique to each system and can be simply described by two parameters: damping constant and natural frequency. Most commonly, a single degree of freedom lumped spring mass system is utilized to study the dynamic characteristics of a vibrating body associated with energy harvesting (Laura et al. 1974). The single degree of freedom helps to study unidirectional

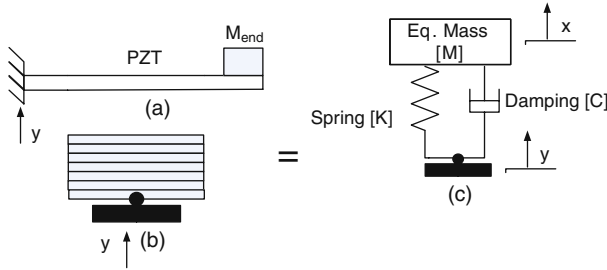


Fig. 1.1 (a) Cantilever beam with tip mass, (b) multilayer PZT subjected to transverse vibration excited at the base, and (c) equivalent lumped spring mass system of a vibrating rigid body

response of the system. Figure 1.1 shows a diagram of a cantilever beam with piezoelectric plates bonded on a substrate and a proof mass at the end; multilayer piezoelectric plates and equivalent lumped spring mass with external excitation. Cantilever structure with tip mass is the most widely used configuration for piezoelectric energy harvesting device. The source of vibration is shown with an arrow at the base of the contact point. The stiffness of the structure depends on the loading condition, material, and cross-sectional area perpendicular to the direction of vibration. The governing equation of motion for the system shown in Fig. 1.1(c) can be obtained from energy balance equation or D'Alembert's principle. This configuration applies to both the energy harvesting mechanisms shown in Fig. 1.1(a) and (b).

The governing equation of motion of a lumped spring mass system can be written as:

$$M\ddot{z} + C\dot{z} + Kz = -M\ddot{y} \quad (1.1)$$

where $z = x - y$ is the net displacement of mass. Equation (1.1) can also be written in terms of damping constant and natural frequency. A damping factor, ζ , is a dimensionless number defined as the ratio of system damping to critical damping as:

$$\zeta = \frac{c}{c_c} = \frac{c}{2\sqrt{mK}} \quad (1.2a)$$

The natural frequency of a spring mass system is defined by Eq. (1.2b) as:

$$\omega_n = \sqrt{\frac{K}{M}} \quad (1.2b)$$

where the stiffness K for each loading condition should be initially calculated. For example, in case of a cantilever beam, the stiffness K is given by $K = 3EI/L^3$, where E is the modulus of elasticity, I is the moment of inertia, and L is the length of beam. The moment of inertia for a rectangular cross-sectional can be obtained from expression, $I = (1/12)bh^3$, where b and h are the width and thickness of

the beam in transverse direction, respectively. For the other cross-sectional area and stiffness, formulas are available in standard mechanical engineering handbook (Blevins, 1979). The power output of piezoelectric system will be higher if system is operating at natural frequency which dictates the selection of material and dimensions. The terms “natural frequency” and “resonant frequency” are used alternatively in literature, where natural frequency of piezoelectric system should not be confused with natural frequency of mechanical system.

The ratio of output $z(t)$ and input $y(t)$ can be obtained by applying Laplace transform with zero initial condition on Eq. (1.1) as:

$$\left| \frac{Z(s)}{Y(s)} \right| = \frac{s^2}{s^2 + 2\zeta\omega_n s + \omega_n^2} \quad (1.3)$$

The time domain of the response can be obtained by applying inverse Laplace transform on Eq. (1.3) and assuming that the external base excitation is sinusoidal given as: $y = Y \sin(\omega t)$:

$$z(t) = \frac{\left(\frac{\omega}{\omega_n}\right)^2}{\sqrt{\left(1 - \left(\frac{\omega}{\omega_n}\right)^2\right)^2 + \left(2\zeta\frac{\omega}{\omega_n}\right)^2}} Y \sin(\omega t - \phi) \quad (1.4)$$

The phase angle between output and input can be expressed as $\Phi = \arctan\left(\frac{C\omega}{K - \omega^2 M}\right)$. The approximate mechanical power of a piezoelectric transducer vibrating under the above-mentioned condition can be obtained from the product of velocity and force on the mass as:

$$P(t) = \frac{m\zeta Y^2 \left(\frac{\omega}{\omega_n}\right)^3 \omega^3}{\left(1 - \left(\frac{\omega}{\omega_n}\right)^2\right)^2 + \left(2\zeta\frac{\omega}{\omega_n}\right)^2} \quad (1.5)$$

The maximum power can be obtained by setting the operating frequency as natural frequency in Eq. (1.5):

$$P_{max} = \frac{mY^2\omega_n^3}{4\zeta} \quad (1.6)$$

Using Eq. (1.6), it can be seen that power can be maximized by lowering damping, increasing natural frequency, mass and amplitude of excitation.

There are two common modes utilized for piezoelectric energy harvesting: 33-mode (stack actuators) and 31-mode (bimorphs). In 33-mode, the direction of applied stress (force) and generated voltage is the same, while in 31-mode the stress is applied in axial direction but the voltage is obtained from perpendicular direction

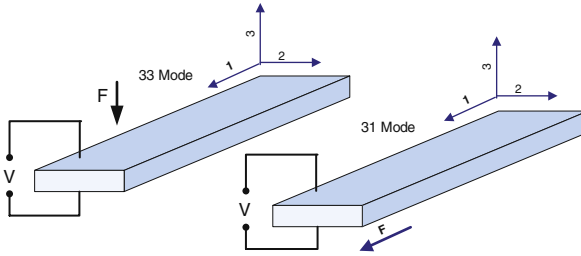


Fig. 1.2 Operating modes of piezoelectric transducer

as shown in Fig. 1.2. For a cantilever beam with long length, the lumped parameter model may not provide reasonable estimate of the output. Contrary to the single degree-of-freedom model (lumped spring mass system), the continuous system has infinite number of natural frequencies and is a logical extension of discrete mass systems where infinite numbers of masses are connected to each other, each having their own degree of freedom.

1.2 Case Study: Piezoelectric Plates Bonded to Long Cantilever Beam with tip mass

Sometimes, small size piezoelectric plates are bonded to a long cantilever beam and need arises to find the stress distribution along the length as a function of excitation frequency. We outline here a simple step-by-step procedure as a starting guideline to find the stress distribution along the continuous beam that can be used to locate the position of piezoelectric plates.

1. Using the governing equation of motion, find the relative displacement which is a function of position and time. The curvature and transverse displacement of a beam can be obtained from the fundamental Euler–Bernoulli beam equation for the given boundary condition expressed as:

$$EI \frac{\partial^4 w(x, t)}{\partial x^4} = -\lambda_m \frac{\partial^2 w(x, t)}{\partial t^2} \quad (1.7)$$

where $\lambda_m = \rho A$ is the linear mass density of the beam.

2. Apply the boundary condition and solve the differential equation. For the cantilever beam of mass M_v and loaded with tip mass M , the boundary conditions are given as:

$$\begin{aligned}
w(0, t) &= \frac{\partial w}{\partial x}(0, t) = 0, \\
\frac{\partial^2 w}{\partial x^2}(L, t) &= 0, \\
El \frac{\partial^3 w}{\partial x^3}(L, t) &= M \frac{\partial^2 w}{\partial x^2}(L, t)
\end{aligned} \tag{1.8}$$

3. Obtain the solution for governing equation using separation of variables method. The general solution for Eq. (1.7) is given as:

$$\begin{aligned}
w_i(x, t) &= \phi(x)q(t) \\
\phi(x) &= C_1 \cos \lambda \frac{x}{L} + C_2 \sin \lambda \frac{x}{L} + C_3 \cos \lambda \frac{x}{L} + C_4 \sin \lambda \frac{x}{L}
\end{aligned} \tag{1.9}$$

4. Apply the boundary condition and solve for unknown C 's. The natural frequency of transversal vibration of a continuous cantilever beam can be obtained analytically from the decoupled equation of Euler–Bernoulli beam and is given by Eq. (1.10) as:

$$f_i = \frac{1}{2\pi} \left(\frac{\lambda}{L} \right)^2 \sqrt{\frac{EI}{\rho A}} \tag{1.10}$$

where i is the mode index, ρ is the mass density, A is the cross-sectional area of beam, and L is the length of the beam.

5. Obtain the solution for forcing term $q(t)$ from equation of motion. The solution of Eq. (1.7) for a cantilever beam of mass $M_v = \rho A$, with a tip mass (M) and boundary condition (Eq. (1.8)), was derived by Erturk and Inman (2007) as follows:

$$w_i(x, t) = \phi(x)q(t) = \omega^2 \sum_{r=1}^{\infty} \frac{\phi(x)(\psi)}{\omega_r^2 - \omega^2 + i2\zeta\omega_r\omega}$$

where

$$\begin{aligned}
\Phi(x) &= C_r \left\{ \cos \left(\frac{\lambda x}{L} \right) - \cosh \frac{\lambda x}{L} - \beta \left[\sin \frac{\lambda x}{L} - \sinh \frac{y_i x}{L} \right] \right\} \\
\beta &= \frac{mL(\sin \lambda - \sinh \lambda) + \lambda M(\cos \lambda - \cosh \lambda)}{mL(\sin \lambda + \cosh \lambda) - \lambda M(\sin \lambda - \sinh \lambda)} \\
q(t) &= \frac{\psi \omega^2}{\omega_r^2 - \omega^2 + i2\zeta\omega\omega_r} y_o e^{j\omega t} \\
\psi &= -m \int_0^L \Phi(x) dx + M_z \Phi(L)
\end{aligned} \tag{1.11}$$

6. The strain ε on surface of beam at a distance y from the neutral axis can be obtained by taking second partial derivative of transverse displacement $w_i(x, t)$:

$$\varepsilon(x) = -y \frac{\partial^2 w}{\partial x^2} \quad (1.12)$$

7. The approximate stress as a function of ratio of distance from the fixed end to the specific location on beam can be obtained from Hooke's law as follows:

$$\sigma(x) = E\varepsilon(x) \quad (1.13)$$

where E is the modulus of elasticity of beam material. If piezoelectric plates are bonded at certain section of a beam, the output voltage from PZT can be estimated by just multiplying the stress at that location with the piezoelectric voltage constant, g . Assuming that the material is linear, elastic, and isotropic with an average stress applied along the 1–1 direction, the output voltage can be determined as follows:

$$V\left(\frac{x}{L}\right) = g_{31} E \varepsilon\left(\frac{x}{L}\right) L_b \quad (1.14)$$

The output power of a PZT at location x from the clamped end and connected to a resistive load can be expressed as:

$$P = \frac{v^2}{R_L} = \frac{1}{R_L} \left\{ g_{31} E \varepsilon\left(\frac{x}{L}\right) L_b \right\}^2 \quad (1.15)$$

where R_L is the load resistance and L_b is the length of piezoelectric crystal bonded to substrate beam.

1.3 Piezoelectric Materials

There are two extreme cases of the high-energy density material, PVDF piezoelectric polymer ($d_{33} = 33$ pC/N, $\varepsilon_{33}/\varepsilon_0 = 13$, $g_{33} = 286.7 \times 10^{-3}$ m²/C), and relaxor piezoelectric single crystals such as PZN – 7%PT ($d_{33} = 2500$ pC/N, $\varepsilon_{33}/\varepsilon_0 = 6700$, $g_{33} = 42.1 \times 10^{-3}$ m²/C). It can be seen from this data that piezoelectric polymer has the highest piezoelectric voltage constant, g_{33} , of 286.7×10^{-3} m²/C and relaxor-based single crystals have the highest product ($d_{33} \cdot g_{33}$) of the order of $105, 250 \times 10^{-15}$ m²/N. However, the synthesis of both single crystal materials and polymers in large volume is challenging and expensive. Thus, for mass applications, current focus is on improving the properties of polycrystalline ceramics. In this section, we will review some of the developments in the synthesis of high-energy density materials covering ceramics, single crystals, polymers, and thin films.

1.3.1 Piezoelectric Polycrystalline Ceramics

A high-energy density material is characterized by the large magnitude of product of the piezoelectric voltage constant (g) and the piezoelectric strain constant (d) given as ($d.g$). The condition for obtaining large magnitude of $d.g$ has been shown to be as $|d| = \varepsilon^n$, where ε is the permittivity of the material and n is a material parameter having lower limit of 0.5. Table 1.1 shows the relationship between magnitude of n and g_{33} for various commercial compositions. It can be clearly seen from this data that as the magnitude of n decreases the magnitude of g_{33} increases. Islam and Priya (2006a, 2006b) have shown that high-energy density piezoelectric polycrystalline ceramic composition can be realized in the system $\text{Pb}(\text{Zr}_{1-x}\text{Ti}_x)\text{O}_3 - \text{Pb}[(\text{Zn}_{1-y}\text{Ni}_y)_{1/3}\text{Nb}_{2/3}]\text{O}_3$ (PZT – PZNN). The compositions investigated in their study can be represented as: $0.9 \text{Pb}(\text{Zr}_{0.52}\text{Ti}_{0.48})\text{O}_3 - 0.1 \text{Pb}(\text{Zn}_{1/3}\text{Nb}_{2/3})\text{O}_3$ [0.9PZT(52:48) – 0.1PZNN] + y wt% MnCO_3 , where y varies from 0 wt% to 0.9 wt% and $0.9 \text{Pb}(\text{Zr}_{0.56}\text{Ti}_{0.44})\text{O}_3 - 0.1 \text{Pb}[(\text{Zn}_{0.8}\text{Ni}_{0.2})_{1/3}\text{Nb}_{2/3}]\text{O}_3$ [0.9PZT (56:44) – 0.1PZNN] + y mol% MnO_2 , where y varies from 1 mol% to 3 mol%. The d_{33}, g_{33} values of the samples having composition 0.9PZT (56:44) – 0.1PZNN + 2 mol% MnO_2 (sintered in two steps at 1100–1000 °C) was found to be as 18, $456.2 \times 10^{-15} \text{ m}^2/\text{N}$. This composition was also found to exhibit a high magnitude of g_{33} as 83.1 V m/N, corresponding to the magnitude of n as 1.126.

Table 1.1 Piezoelectric properties and energy harvesting parameter of various commercially available piezoelectric ceramic materials (Copyright: Blackwell Publishing)

Composition	$\varepsilon_{33}/\varepsilon_0$	d_{33} (pC/N)	g_{33} (V m/N)	$d_{33}.g_{33}$ (m^2/N)	n
Morgan electroceramics					
PZT 701	425	153	41×10^{-3}	6273×10^{-15}	1.165
PZT 703	1100	340	30×10^{-3}	10200×10^{-15}	1.181
PZT 502	1950	450	25×10^{-3}	11250×10^{-15}	1.204
PZT 507	3900	700	20×10^{-3}	14000×10^{-15}	1.227
American Piezoelectric Ceramics International					
APC 880	1000	215	25×10^{-3}	5375×10^{-15}	1.20
APC 840	1250	290	26.5×10^{-3}	7685×10^{-15}	1.198
APC 841	1350	300	25.5×10^{-3}	7650×10^{-15}	1.202
APC 850	1750	400	26×10^{-3}	10400×10^{-15}	1.203
APC 855	3400	620	21×10^{-3}	12600×10^{-15}	1.224
Ferroperm Piezoceramics					
Pz 24	400	190	54×10^{-3}	10260×10^{-15}	1.150
Pz 26	1300	300	28×10^{-3}	8400×10^{-15}	1.199
Pz 39	1780	480	30×10^{-3}	14400×10^{-15}	1.194
Pz 52	1900	420	25×10^{-3}	10500×10^{-15}	1.206
Pz 29	2900	575	23×10^{-3}	13225×10^{-15}	1.217
Edo Corporation					
EC-63	1300	295	24.1×10^{-3}	7109.5×10^{-15}	1.20
EC-65	1725	380	25×10^{-3}	9500×10^{-15}	1.205
EC-70	2750	490	20.9×10^{-3}	10241×10^{-15}	1.222
EC-76	3450	583	19.1×10^{-3}	11135.3×10^{-15}	1.228

The selection of piezoelectric ceramic composition for a particular application is dependent on parameters such as operating temperature range ($-20 \leq T \leq 80^\circ\text{C}$), operating frequency range (10–200 Hz), external force amplitude (0.1–3N), and lifetime ($>10^6$ cycles). The operating temperature range is determined by the Curie temperature of material which for most of the $\text{Pb}(\text{Zr}, \text{Ti})\text{O}_3$ ceramics is greater than 200°C .

Recently, there has been emphasis on utilizing lead-free materials in domestic and medical applications. Out of all the possible choices for lead-free ceramics, $(\text{Na}, \text{K})\text{NbO}_3$ (KNN)-based ceramics such as KNN-LiNbO_3 , KNN-LiTaO_3 , KNN-LiSbO_3 , $\text{KNN-Li}(\text{Nb}, \text{Ta}, \text{Sb})\text{O}_3$, KNN-BaTiO_3 (BT), KNN-SrTiO_3 , and KNN-CaTiO_3 have gained prominence mainly for two reasons: (i) piezoelectric properties exist over a wide range of temperature and (ii) there are several possibilities for substitution and additions. Table 1.2 lists some of the prominent lead-free compositions based on KNN and $(\text{Na}_{1/2}\text{Bi}_{1/2})\text{TiO}_3$ (NBT) – $(\text{K}_{1/2}\text{Bi}_{1/2})\text{TiO}_3$ (KBT) (Shrout and Zhang 2007, Guo et al. 2004, Yuan et al. 2006, Takenaka and Nagata 2005, Zhao et al. 2007, Zang et al. 2006, Ming et al. 2007, Park et al. 2006, Ahn et al. 2007, Cho et al. 2007). NBT-KBT-based ceramics suffer from drawback that there is anti-ferroelectric phase transition at low temperatures that limits the operating range of transducers. Alkali niobate-based ceramics are currently being commercialized by several companies in Europe and Japan and are expected to be available in large quantities in near future.

1.3.2 Piezoelectric Single Crystal Materials

Oriented single crystals of $(1-x)\text{Pb}(\text{Zn}_{1/3}\text{Nb}_{2/3})\text{O}_3 - x\text{PbTiO}_3$ (PZN-PT) and $(1-x)\text{Pb}(\text{Mg}_{1/3}\text{Nb}_{2/3})\text{O}_3 - x\text{PbTiO}_3$ (PMN-PT) have been reported to have exceptional properties, such as longitudinal electromechanical coupling factors of 0.95 (Kuwata et al. 1981, 1982; Park and Shrout 1997a, 1997b, 1997c), longitudinal piezoelectric coefficients between 1500 and 2500 pC/N (Kuwata et al. 1981, 1982; Park and Shrout 1997a, 1997b, 1997c;), and electrically induced strains of up to 1.7% (Park and Shrout 1997a, 1997b, 1997c). Single crystals of PZN-PT are grown

Table 1.2 Summary of the lead-free compositions based on KNN system

System	d_{33} (pC/N)	ϵ_3^T/ϵ_o	$\tan \delta$	k_p	$T_d/T_c(^{\circ}\text{C})$
NBT-KBT-BT	183	770	0.03	0.37	100/290
NBT-KBT-LBT	216	1550	0.03	0.40	160/350
KNN–LiNbO ₃	235	500	0.04	0.42	–/460
KNN–LiTaO ₃	268	570	0.01	0.46	–/430
KNN–LiSbO ₃	283	1288	0.02	0.50	–/392
KNN–Li(Nb,Ta,Sb)O ₃	308	1009	0.02	0.51	–/339
KNN–BaTiO ₃	225	1058	0.03	0.36	–/304
KNN–SrTiO ₃	220	1447	0.02	0.40	–
KNN–CaTiO ₃	241	1316	0.09	0.40	–/306

T_d : depolarization temperature; T_c : Curie temperature.

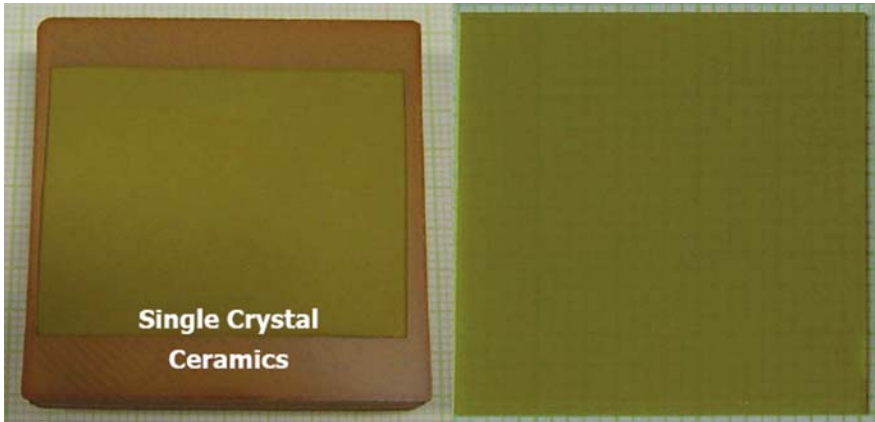


Fig. 1.3 A schematic of the PMN-PZT single crystal synthesized through solid-state crystal growth technique (Copyright: Ho-Yong Lee, Ceracomp Co., Ltd.)

widely using self-flux method (Koyabashi et al. 1997; Mulvihill et al. 1996) while that of PMN-PT by Bridgman's technique (Commercial suppliers such as H. C. Materials Corporation, TRS Technologies, and IBULE Photonics).

Recently, Lee et al. have shown the possibility of synthesizing large size crystals through solid state conversion process as shown in Fig. 1.3 (Ceracomp Co. Ltd.). In this method, a seed crystal is bonded to the surface of the ceramic compact or embedded in the powder compact and the composite sample is carefully sintered at high temperatures. Table 1.3 lists the properties of $\text{Pb}(\text{Mg}_{1/3}\text{Nb}_{2/3})\text{O}_3 - \text{PbTiO}_3$ (PMN-PT) crystals grown by Bridgman's technique and PMN-PZT by solid-state conversion. Clearly, the system PMN-PZT offers higher rhombohedral–tetragonal transition temperature (T_{R-T}) extending the operating range of the transducer.

The piezoelectric coefficients of single crystal can be enhanced by special cuts and poling as shown in Fig. 1.4 (Zhang et al. 2004). This is quite useful for designing the bimorph-type transducer structures, which mainly utilize d_{31} or d_{32} coefficients. A simple vibration energy harvesting device using d_{32} -mode piezoelectric single crystals can be designed as shown in Fig. 1.5. The structure consists of unimorph- or bimorph-type transducers with single crystal plates bonded on one side or both sides of the metal plates (e.g., brass and aluminum). The transducers are rigidly

Table 1.3 Properties of $\langle 001 \rangle$ oriented piezoelectric single crystals available through commercial sources

Material	T_c (°C)	T_{R-T} (°C)	d_{33} (pC/N)	ϵ_{33}/ϵ_0	\tan^{TM} (%)	k_{33}
PMN-PT-B (HC Material)	–	~75	2000–3500	5500–6500	0.8	0.90–0.94
TRS-X2C (TRS Tech.)	160	75	2200–2700	6500–8500	1	0.92
Type IB (Ibule Ph.)	–	88	1871	6502	< 1	0.91
70PMN-30PT (Ceracomp)	130	90	1500	5000	< 1	0.9
CPSC20-130 (Ceracomp)	195	130	1450	4200	< 1	0.9

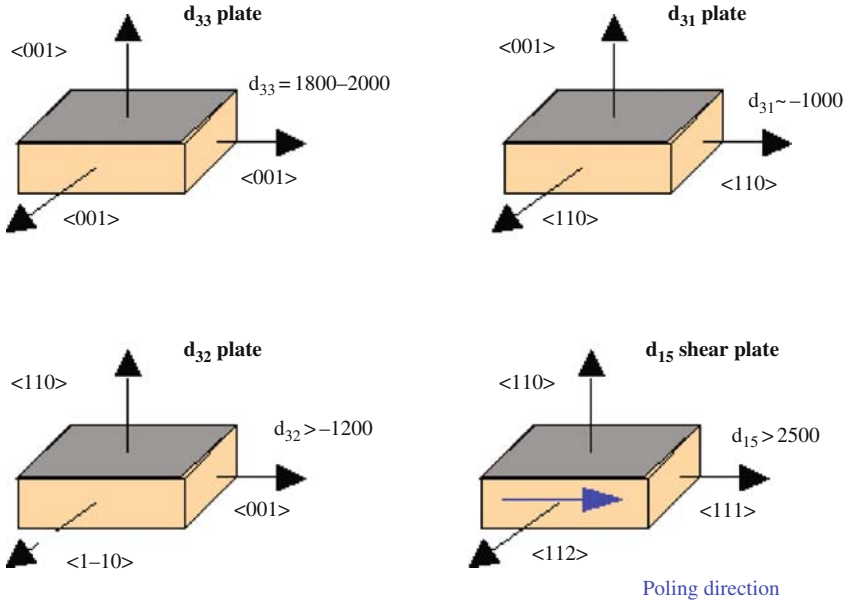


Fig. 1.4 Variation in the piezoelectric coefficients with orientation and poling direction (Copyright: TRS Technologies, State College, PA 16801)

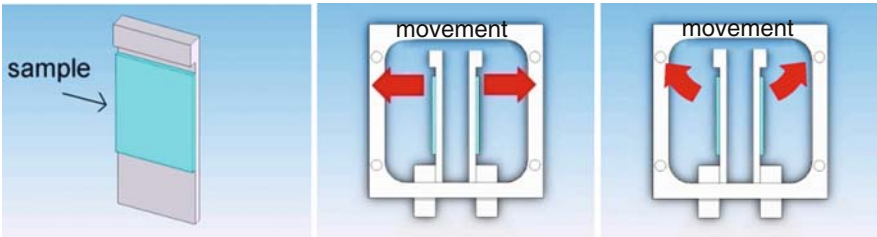


Fig. 1.5 Schematic representation of a bimorph transducer-based uniaxial energy harvester. The operating frequency is tuned by the material and dimensions of the beam and tip mass

fixed in a small cubical box with freedom to oscillate in a specific direction. The tip mass, material for beam, and dimensions of beam determine the operating frequency which could be matched with the resonance frequency of the system. The advantage of bimorph-based devices is that they are simple to fabricate and cheap. The disadvantage is that they are uniaxial systems and limited in power density.

1.3.3 Piezoelectric and Electrostrictive Polymers

Polyvinylidene fluoride (PVDF) is a semi-crystalline high-molecular weight polymer with repeat unit (CH₂-CF₂), whose structure is essentially head-to-tail,